International Journal of Nanomedicine

Dovepress
Taylor & Francis Group

Open Access Full Text Article

ORIGINAL RESEARCH

RGD-Functionalized Ginsenoside Rg3 Liposomes for Alleviating Oxidative Stress and Choroidal Neovascularization in Age-Related Macular Degeneration

Jie Zhou[1,*], Dengminghong Zhao[1,*], Shaotian Niu[2], Weiwei Meng[1], Zhoujiang Chen[1], Hanmei Li[3], Ya Liu[2,4], Liang Zou[3], Wei Li[2,5]

[1]School of Pharmacy, Chengdu University, Chengdu, 610106, People's Republic of China; [2]State Key Laboratory of Southwestern Chinese Medicine Resources, School of Pharmacy, Chengdu University of Traditional Chinese Medicine, Chengdu, 611137, People's Republic of China; [3]School of Food and Biological Engineering, Chengdu University, Chengdu, 610106, People's Republic of China; [4]Affiliated Hospital & Clinical Medical College of Chengdu University, Chengdu University, Chengdu, 610081, People's Republic of China; [5]School of Basic Medicine, Chengdu University, Chengdu, 610106, People's Republic of China

*These authors contributed equally to this work

Correspondence: Liang Zou, School of Food and Biological Engineering, Chengdu University, No. 2025 Chengluo Avenue, Chengdu, 610106, People's Republic of China, Email zouliangcdu@126.com; Wei Li, School of Basic Medical Sciences, Chengdu University, No. 2025 Chengluo Avenue, Chengdu, Sichuan, 610106, People's Republic of China, Email liweicdu@126.com

Background and Aim: Age-related macular degeneration (AMD) is a leading cause of vision loss owing to choroidal neovascularization (CNV) and retinal vascular abnormalities. Current anti-VEGF therapies often exhibit limited efficacy in approximately 50% of patients owing to the complex pathological microenvironment, including elevated reactive oxygen species (ROS) levels. This study aimed to develop a multitargeted therapeutic strategy for AMD by leveraging the antioxidant and anti-angiogenic properties of ginsenoside Rg3 (Rg3).

Methods: RGD-Rg3@Lips was formulated to encapsulate Rg3 and modified with (Arginine-Glycine-Aspartic Acid, RGD) peptides for targeted delivery. In vitro studies have evaluated the cellular internalization, anti-angiogenic effects, and suppression of oxidative stress and inflammation in ARPE-19 cells. In vivo efficacy was assessed using a laser-induced AMD mouse model, in which an intravitreal injection of RGD-Rg3@Lips was administered. Mechanistic studies have focused on the hypoxia-inducible factor 1-α, (HIF-1α) / vascular endothelial growth factor, (VEGF) signaling pathway and the expression of inflammatory cytokines.

Results: RGD-Rg3@Lips demonstrated superior cellular internalization and anti-angiogenic efficacy compared to Rg3@Lips and free Rg3 in vitro, significantly reducing oxidative stress and inflammation. In vivo, RGD-Rg3@Lips markedly reduced CNV formation and vascular leakage in an AMD mouse model. Mechanistically, RGD-Rg3@Lips attenuated oxidative stress, inhibited the HIF-1α/VEGF pathway, and downregulated key inflammatory cytokines including tumor necrosis factor α (TNF-α) and VEGF. RGD modification significantly improved the targeting of CNV lesions, enhancing therapeutic efficacy by specifically binding to vascular surface integrin receptors compared to non-modified liposomes and free Rg3.

Conclusion: This study highlights the potential of RGD-Rg3@Lips as a novel multitargeted therapeutic strategy for wet AMD. By combining the antioxidant and antiangiogenic properties of Rg3 with targeted drug delivery, RGD-Rg3@Lips offers a promising approach to address the limitations of current AMD therapies. These findings underscore the value of natural-product-based nanomedicine for the treatment of complex ocular diseases.

Keywords: multitargeted therapeutic, ginsenoside Rg3, choroidal neovascularization, CNV, age-related macular degeneration, AMD, oxidative stress

Received: 28 February 2025
Accepted: 9 June 2025
Published: 19 June 2025

Graphical Abstract

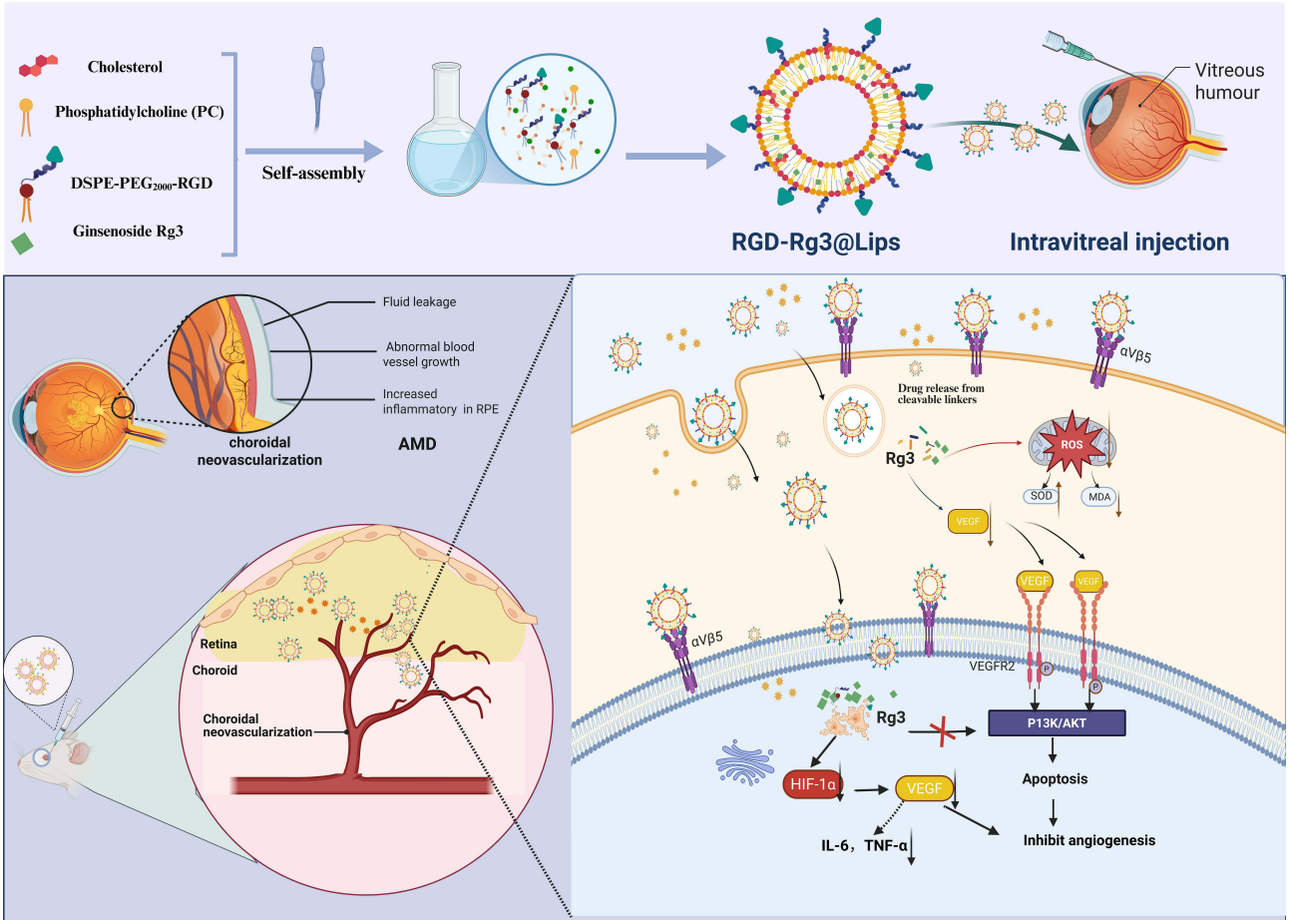

Introduction

Age-related macular degeneration (AMD) is a progressive and degenerative disease that affects the macular region of the retina and is a major cause of irreversible vision loss in the elderly population. It is estimated that by 2040, the global prevalence of AMD will rise to 1.5 × its 2020 level, reaching approximately 288 million individuals, and AMD has become the third leading cause of blindness globally, following glaucoma and cataracts.[1] Meanwhile, research has reported that the number of patients with AMD in China is expected to reach 55.19 million by 2050.[2] Clinically, this disease is classified into two types based on the pathological features of the macula: non-exudative geographic atrophy (dry AMD) and exudative choroidal neovascularization (wet AMD).[3] Although only 10–15% of patients are diagnosed with wet AMD, it accounts for almost all the rapid loss of central vision and permanent visual impairment in the population, with significant impacts on quality of life.[4] Multiple pathogenic factors, including gene expression, age, inflammatory environment, oxidative stress and neovascularization.[5–7] Choroidal neovascularization (CNV) is a major cause of wet AMD. Currently, the most effective treatment for CNV is intravitreal injections of anti-vascular endothelial growth factor (VEGF) antibodies (aV), such as bevacizumab, ranibizumab, aflibercept, and faricimab.[8–10] However, their therapeutic efficacy remains limited, with approximately 40% of patients showing resistance to aV treatment and an incomplete response even after one year of continuous treatment, which may be due to inefficient delivery of aV to the fundus as well as the complex pathogenesis of wet AMD.[11] Moreover, Patients are subjected to frequent drug administration and multiple invasive intravitreal injections, which leads to many complications such as ocular

hemorrhage, infection, retinal detachment, and increased intraocular pressure.[12] Therefore, multi-targeted therapeutic agents and efficient drug delivery methods remain major goals in AMD therapeutic drug research.

In recent years, both clinical and preclinical studies have reported that inflammation is an important cause of AMD development, not only because of neovascularization but also as a driver of CNV.[13] Therefore, several glucocorticoids have been used to treat ocular inflammation or edema associated with AMD in order to counteract the inflammatory environment associated with ocular neovascularization. Glucocorticoids can induce ocular hypertension and increase the risk of glaucoma and cataracts.[14] Recently, various herb-derived natural anti-inflammatory and antioxidant products have been demonstrated to be effective in treating AMD, such as quercetin,[15] astaxanthin,[16] and lutein.[17] Ginsenoside Rg3 (Rg3), the main active ingredient of the traditional Chinese medicine ginseng, has the pharmacological effects of anti-oxidation, anti-inflammatory, anti-angiogenesis, anti-tumor and immune-enhancement.[18–21] Studies have shown that Rg3 liposomes (lips) can effectively locate in the retinal pigment epithelium (RPE) layer and ameliorate retinal ischemia-reperfusion (RIR) injury by downregulating pro-inflammatory factors and regulating macrophage polarization in the retinal microenvironment.[22] Moreover, Rg3 has been shown to interferes with the development of diabetic retinopathy by downregulating the expression of VEGF and tumor necrosis factor α (TNF-α) in the retina.[23] Therefore, Rg3 can be used as a potential therapeutic agent for AMD owing to its dual antiangiogenic and antioxidant effects. However, the tight physiological barrier in the eye limits the efficiency of Rg3 delivery to the posterior segment of the eye.

While polymer- and lipid-based nanocarriers have emerged as promising strategies for ocular drug delivery, challenges such as insufficient targeting specificity and rapid clearance in the vitreous remain unresolved.[24] Recent advances in supramolecular engineering, exemplified by nanoceria systems that block oxidative stress through dual-level mechanisms, highlight the importance of multifunctional designs for AMD therapy.[25] Additionally, bioactive hydrogels inspired by biological systems have demonstrated potential in corneal repair by enhancing drug retention and cellular interaction, yet their application in posterior segment disorders like AMD remains unexplored.[26] To address these limitations and problems, we designed arginine-glycine-aspartate (RGD) peptide-modified liposomes to promote the accumulation of Rg3 in the retina and expected to enhance the therapeutic effect. It has been reported that RPE uses integrin $\alpha v\beta_5$ to recognize and remove the outer segment of the photoreceptor that is detached from the retina. $\alpha_v\beta_5$ integrin receptor plays an important role in retinal function and RPE.[27,28] RGD peptides specifically bind to integrin receptors.[29,30] Therefore, RGD peptide can be used as a target for drug delivery to accurately achieve targeted drug delivery.[31] Moreover, the integrin receptor $\alpha_v\beta_3$ is overexpressed on the surface of CNV during ocular neovascularization.[32–34] Based on this combination, RGD peptides that specifically target integrin receptors have been developed to actively target nanoparticles delivered to the retinal region, thereby increasing drug concentration in the posterior segment of the eye to play a therapeutic role.

In this study, we constructed RGD peptide-modified lips and encapsulated Rg3 (RGD-Rg3@ Lips) in targeted CNV therapy. The cytotoxicity of RGD-Rg3@ Lips on a human retinal pigment epithelial cell line (ARPE-19) and human umbilical vein endothelial cells (HUVECs) and their targeting ability in vitro and in vivo were evaluated. The in vitro anti-vascular effect was evaluated using tube formation and wound healing tests. The therapeutic effect of the laser-induced CNV mouse model was evaluated by hematoxylin and eosin (HE) staining, choroid stretched preparation, and enzyme-linked immunosorbent assay (ELISA) detection of inflammatory factors in tissues. To the best of our knowledge, this is the first study on RGD-modified Lips encapsulating Rg3 for angiogenesis therapy in laser-induced CNV mouse models. This lays the foundation for the application of Rg3 in ocular diseases and provides a new approach to AMD treatment.

Materials and Methods

Materials, Cells and Animals

Ginsenoside Rg3 (>97%) was purchased from Sichuan Weikeqi Biological Company (Sichuan, China), DSPE-PEG_{2000}-RGD and DSPE-PEG_{2000} were from Xi'an Ruixi Biological Technology (Xi'an, China), DiD (Far-red Plasma Membrane Fluorescent Probe) and coumarin-6 (C_6) were obtained from Shanghai Yuanye Bio- Technology (Shanghai, China), and cholesterol was from Dalian Meilun Biotechnology (Dalian, China). Soybean lecithin (PC) was purchased from the

Shanghai Yuanye Biological Company (Shanghai, China). Human umbilical vein endothelial cells (HUVECs) were obtained from Invitrogen (Carlsbad, CA, USA) and cultured in Dulbecco's Modified Eagle Medium (DMEM) (Gibco, USA) supplemented with 10% fetal bovine serum (FBS) (Zhejiang Tianhang Bio-technology Co., China), 100 U/mL penicillin, and 100 μg/mL streptomycin (Wuhan boster Bio-engineering Co., China) in a humidified incubator at 37 °C in an atmosphere containing 5% CO_2. Human retinal pigment epithelial (ARPE-19) cells were obtained from ProCell (Wuhan, China). The cells were cultured in DMEM/F-12 medium (Procell, China) containing 10% FBS, penicillin (100 U/mL), and streptomycin (100 μg/mL) at 37 °C in a humidified incubator with 5% CO_2. Male C57BL/6 mice (6–8 weeks old) were supplied by Chengdu Dashuo Biotechnology (Chengdu, China). Mice had free access to food and water and were housed in a temperature-controlled barrier facility under a 12-h light/dark cycle. All animal experiments were approved by the Institutional Animal Care and Ethics Committee of Chengdu University.

Preparation and Characterization of Lips

RGD-Rg3@Lips and other Lips were prepared using a thin-film ultrasound. Briefly, accurately quantities of soya bean lecithin (SPC), cholesterol (Chol), DSPE-PEG_{2000}, DSPE-PEG_{2000}-RGD, and Rg3, in a mass ratio of 6:24:1:2:6, were dissolved in a 6 mL of methanol/chloroform mixture (1:1, v/v). The solution was then sonicated thoroughly and transferred into a 50 mL eggplant-shaped flask. The solvent was subsequently evaporated under vacuum at 40 °C, resulting in a uniform and transparent lipid film that was hydrated with phosphate-buffered saline (PBS pH 7.4). RGD-Rg3@Lips and Rg3@Lips were formed by sonication using a probe ultrasonic instrument (Ymnl-1000Y, Ultrasonicator, China) at 600 W for 3 s per cycle in an ice water bath.

The particle size distribution and zeta potential of Rg3@Lips and RGD-Rg3@Lips were measured in triplicate using a dynamic light scattering (DLS) instrument (Brookhaven, Instruments-Omni, USA). The morphology of lips was observed by staining samples with 2% phosphotungstic acid and subsequently analyzing them by transmission electron microscopy (TEM; JEM-1200 EX, Japan) at an accelerating voltage of 100 kV. The drug-loading (DL) capacity and entrapment efficiency (EE) of Rg3 within the lips were quantified by ultrafiltration centrifugation. Specifically, 1 mL of Rg3 loaded Lips solution was added to an ultrafiltration tube (10000 Da, Millipore, USA) and centrifuged at 4 °C and 7500 rpm for 30 min. The upper layer was collected and the lips were demulsified with methanol. The resultant solution was then analyzed for Rg3 contents by using High-performance liquid chromatography (HPLC, Shimadazu, SIL-16, China). The HPLC conditions were as follows: a Welchrom-C_{18} column (250 × 4.6 mm, 5 μm) was used to determine the concentration and entrapment efficiency of Rg3 in the Lips; the mobile phase consisted of acetonitrile and water (55:45, v/v); the injection volume was 20 μL; the flow rate was 1.0 mL/min; and the detection wavelength was set at 203 nm. The concentration of Rg3 in the Lips was determined using a standard curve.

EE (%) = encapsulated Rg3 amount/total Rg3 amount × 100%

DL (%) = encapsulated Rg3 amount/total lipid amount × 100%

The in vitro release study of the lips was conducted over a 48-hour period utilizing the dialysis method. Briefly, 0.5 mL of Rg3, Rg3@Lips, and RGD-Rg3@Lips (at a concentration of 1 mg/mL in Rg3) were introduced into a dialysis bag with a molecular weight cut-off of 12,000 Da. The dialysis membranes were then submerged in 50 mL of simulated artificial vitreous solution containing 2% Tween 80, maintained under continuous agitation at 100 r/min and and at a temperature of 37 °C. Aliquots of the external medium (0.5 mL) were collected at intervals of 1, 2, 4, 6, 8, 12, 24, and 48 h. To maintain the sink conditions, the release medium was replenished after each sampling. The collected samples were diluted with methanol to a final volume of 1 mL and the amount of Rg3 released was quantified using HPLC.

Cell Cytotoxicity Assessment

To assess cytotoxicity, ARPE-19 cells or HUVECs in logarithmic growth phase were seeded into a 96-well plate. After the cells were attached to the plate, the culture medium was removed and replaced with different concentrations of Rg3, Rg3@Lips, and RGD-Rg3@Lips, each diluted in serum-free culture medium. After 24 h of incubation, cell viability was determined for each group using the CCK-8 assay.

In vitro Cellular Uptake

The cellular uptake of free C6, C6@Lipss, and C6@RGD-Lips in ARPE-19 cells was evaluated using flow cytometry (FCM; FACS Verse, BD Biosciences, USA) and confocal laser scanning microscopy (CLSM; TCS SP8, Leica, Germany). Spread, well-growing ARPE-19 cells were cultured in 6-well plates, and free C6, C6@Lips, and C6@RGD-Lips were prepared using coumarin 6 instead of Rg3. These formulations were incubated with cells separately for 4 h. Subsequently, the cells were harvested and suspended in PBS, and intracellular fluorescence signals were analyzed using FCM or CLSM.

Wound Healing Assay

HUVECs were uniformly seeded into 24-well plates. A single clear linear scratch was made in the center of the cell monolayer using a 1 mL pipette. Initial images were captured at 0 h, after which the cells were treated with varying concentrations of Rg3, Rg3@Lips, and RGD-Rg3@Lips. Untreated cells were used as controls. After 24 h of incubation, wound closure was assessed by measuring scratch widths, and migration rates were calculated. Cell migration images were obtained using an optical microscope. The experiments were performed in triplicate to ensure reliability of the results.

Tube Formation Assay

Tube formation assays are often used to validate the anti-angiogenic effects of drugs in vitro following established protocols. Matrigel was initially stored at −20 °C and then thawed to a liquid state at 4 °C overnight. The Matrigel was then dispensed into a 96-well plate using a pre-cooled pipette tip and allowed to solidify at 37 °C for 45 min. HUVECs were seeded on a Matrigel matrix. Rg3 (80 μM), Rg3@Lips, and RGD-Rg3@Lips were administered immediately, while untreated cells served as controls. After 4 h of incubation, endothelial tube formation was observed under a microscope and the number of blood vessels and nodes was quantitatively analyzed.

Anti-Oxidative Stress in vitro

ARPE-19 cells in the logarithmic growth phase were seeded in a 96-well plate at a density of 1×10^4 cells/well. After overnight incubation, the spent medium was removed and fresh medium was added to the control wells. The remaining wells were treated with 100 μL of a 6 mm sodium iodate ($NaIO_3$) solution. After a 12 h incubation period, 100 μL of Rg3, Rg3@Lips, or RGD-Rg3@Lips solution, each containing 25 μM Rg3, was added to each well. After a further incubation for 12 h, the cells were exposed to 10 μM DCFH-DA in serum-free culture medium at 37 °C for 30 min. The cells were then washed with PBS, and the fluorescence intensity of DCF in the different samples was measured using a microplate reader (Synergy H1, BioTek, USA) and observed using fluorescence microscopy. The supernatant was collected for malondialdehyde (MDA), superoxide dismutase (SOD), and VEGF analysis according to the MDA/SOD assay kit (Nanjing Jiancheng, China) and VEGF ELISA kit (Elabscience Biotechnology Co., Ltd).

Western Blot (WB) Analysis

Whole cell proteins were extracted from HUVECs treated with different formulations using RIPA lysate (with prior addition of PMSF and phosphatase inhibitors), centrifuged, supernatants extracted, and protein concentrations quantified using the BCA assay from Beyotime. The protein samples (20 μg) were subjected to SDS-PAGE using a precast Tris-HCl gel, then transferred to a PVDF membrane and blocked with 5% skimmed milk for 2 h. Primary antibodies were then added and incubated overnight at 4 °C, and then the membranes were washed with TBS-T and incubated with the corresponding secondary antibodies for 2 h at room temperature. Protein blots were visualized using an ECL Plus Western Blotting Detection System (Tanon-4200SF, Tanon, China). The following primary antibodies were used: PI3K (1:1000, #4257, CST), p-PI3K (1:1000, #4228, CST), AKT (1:1000, #4691, CST), p-AKT (1:2000, #4060, CST), and VEGF (1:1000, ab214424, Abcam). Band intensities were quantified using ImageJ software and normalized to internal control proteins.

Intraocular Distribution and Accumulation

A single intravitreal injection (IVT) study was performed to assess the localization and distribution of lips within the retina. Following the induction of deep anesthesia and pupil dilation, 4 μL of free C6, C6@Lips, and RGD-C6@Lips were injected, each at a C6 concentration of 20 $\mu g\ mL^{-1}$. Mice were euthanized at 2 and 4 h post-injection, and their eyeballs were immediately snap-frozen in optimal cutting temperature (OCT) compound. Subsequently, retinal sections were cut to a thickness of 7 μm using a cryostat microtome (Leica CM1860, Leica Biosystems, Germany). The sections were stained with DAPI and examined under a fluorescence microscope.

Laser-Induced Mouse Choroidal Neovascularization (CNV) Model

A mouse CNV model was established using laser photocoagulation following the methodology previously established in our laboratory.[15] By targeting the Bruch's membrane with a laser pulse, proliferating blood vessels in normal choroidal tissue were able to penetrate the compromised Bruch's membrane and extend into the RPE layer, thereby manifesting the pathological characteristics of CNV. Specifically, Male C57BL/6 mice (aged 6–8 weeks, weighing 18–20 g) were anesthetized by intraperitoneal injection of 1% pentobarbital. Following anesthesia, the pupils were dilated using topical tropicamide. The mice were then positioned on a platform using a slit-lamp. Laser photocoagulation was performed on the right eye of each mouse using a 532 nm laser (Lumenis, Santa Clara, CA, USA) with a power setting at 260 mW, an exposure time of 0.05 seconds, and a spot diameter of 50 μm. Laser burns were applied at the 3, 6, 9, and 12 o'clock positions, with approximately 1–2-disc diameters around the optic disc. The appearance of bubble-like burns in the fundus, indicating rupture of Bruch's membrane, signified successful laser photocoagulation.

In vivo CNV Targeting of Lips

Male C57BL/6 mice that received laser-induced CNV for 14 days were used to evaluate the CNV targeting. These mice received IVT injections of 4 μL free DiD, DiD@Lips, and RGD-DiD@Lips. Choroidal flat mounts were prepared at 2 and 4 h after injection. The RPE/choroid/sclera complexes were incubated overnight at 4°C with Alexa Fluor 488-labelled isolectin GS-IB4 at a 1:100 dilution. Colocalization analysis of the lips at the lesion site was performed using fluorescence microscopy.

Quantification of CNV

After laser modelling, we injected 4 μL of Rg3, Rg3@Lips, or RGD-Rg3@Lips (Rg3 concentration of 3 mg/mL) into the vitreous cavity of experimental eyes of CNV mice (six mice per group) to assess the therapeutic effects. Blank and model groups were injected with the same volume of physiological saline. Due to the acute nature of the laser-induced mouse CNV model, neovascularization typically occurs between the 7th and 14th day after laser injury. Seven days after the laser injury, the mouse eyeballs were fixed in an eye fixative for 1 h, and after removal of the anterior segment, vitreous body, and anterior segment of the retina, a flat choroidal stent was prepared. The laser spot left by the laser was located, centered on the optic nerve and cut radially into a "petal shape" along the 4 laser points, placed in 0.1% Triton permeabilized membrane for 15 min and then transferred to 3% BSA for 3 h. The tissues were incubated with Alexa Fluor488-labelled isolectin GS-IB4 (1: 100) incubated overnight at 4°C, then washed three times with PBS, placed on slides with a drop of anti-fluorescence quencher, sealed, observed, and photographed under a fluorescence microscope, and the area of the CNV area was counted using ImageJ.

Cytokine Levels in Ocular Tissue

After a seven-day modelling period, the mice were divided into four groups: model group and different treatment groups. The treatment groups received IVT injections of 4 μL of Rg3, Rg3@Lips, or RGD-Rg3@Lips every two days for a total of four injections. Subsequently, six eyes from each group were harvested and a ninefold volume of ice-cold PBS was added. The samples were homogenized, and the supernatant was collected after low-temperature centrifugation. The levels of VEGF, TNF-α, IL-6, and HIF-1α in the ocular tissues of different groups were quantified using a murine ELISA kit (Elabscience Biotechnology Co., Ltd).

Hematoxylin and Eosin (HE) Staining

Histopathological analysis of CNV lesions was conducted 7 days after IVT injection. euthanasia, the eyeballs were enucleated and preserved in FAS eye fixative, whereas systemic organs, including the heart, liver, spleen, lungs, and kidneys, were fixed in 4% paraformaldehyde overnight. After rehydration with graded ethanol, the tissues were embedded in paraffin, sectioned at a thickness of 3 μm, stained with hematoxylin and eosin (H&E), and mounted with neutral gum. Microscopic examination of the CNV lesions was performed, and the areas were quantified using ImageJ software.

Statistical Analysis

Statistical analysis was statistically analyzed using one-way analysis of variance in GraphPad Prism 10 software, and all data were expressed as mean ± standard deviation (SD); $p < 0.05$, $p < 0.01$, $p < 0.001$ and $p < 0.0001$ were considered statistically significant.

Results and Discussion

Preparation and Characterization of Lips

As reported in previous studies,[35] Rg3@Lips and RGD-Rg3@Lips were fabricated using the thin-film ultrasonic method. First, the encapsulation process was optimized by a one-way test, considering variables such as phospholipid/cholesterol ratio, drug/lipid ratio, DSPE-PEG_{2000} dosage, sonication power, and time. The optimal lip-preparation process was determined based on the preliminary experimental results. The optimized samples were then prepared and analyzed in triplicate.

According to the optimized formulation, the DL% of Rg3@Lips and RGD-Rg3@Lips were 18.27% and 16.65%, respectively, while the average EE% was 97.2% and 88.35%. As shown in Figure 1A, Rg3@Lips and RGD-Rg3@Lips exhibited uniform spherical morphologies with bilayer membrane structure. DLS measurements revealed that the particle size of Rg3@Lips increased from 90.32 ± 0.84 nm to 98.98 ± 4.03 nm after RGD modification. The corresponding size distribution histograms of lips are shown in Figure 1B. This 9 nm increase in diameter is likely due to surface modification with RGD ligands. The polydispersity indices (PDI) of Rg3@Lips and RGD-Rg3@Lips remained stable at 0.23 ± 0.012 and 0.22 ± 0.005, respectively. Notably, compared to particle size, surface charge has been reported to be a more critical factor influencing nanoparticle delivery to the retina following IVT administration.[36] Specifically, negatively charged nanoparticles have been shown to penetrate the choroid and retina more effectively than cationic nanoparticles do. In this study, the zeta potentials of Rg3@Lips and RGD-Rg3@Lips was −38.45 ± 0.12 and −38.39 ± 0.45 mV, respectively, as shown in Figure 1C. Additionally, stability of Lips was assessed for 15 days at 4 °C by monitoring changes in particle size and PDI. Under these conditions, no statistically significant variations were observed in any of the nanoformulations compared with the initial values (Figure 1D).

The in vitro release profile of the Lips was evaluated by quantifying the cumulative Rg3 release. As illustrated in Figure 1E, the Rg3 exhibited a rapid release behavior within the initial 6 h, with approximately 80% drug released in less than 24 h. In contrast, drug release from the Lips group showed a significant sustained release profile. Previous studies have indicated that Rg3 possesses a steroid-like structure characterized by both hydrophilic glycoside chains and hydrophobic aglycones.[37] This unique structural composition enables Rg3 to interact with phospholipids, allowing it to be embedded in the lipid bilayer structure and to modulate membrane micropolarity and fluidity. Consequently, the unique cholestane-like structure of Rg3 facilitates its encapsulation within the lipid bilayer of the Lips and integration into the lipid membrane. This adaptability makes Lips a more suitable carrier for Rg3, facilitating a high encapsulation efficiency and promoting prolonged in vitro release.

In vitro Cellular Uptake by HUVECs and ARPE-19 Cells

Prior to conducting the in vitro cellular uptake studies, we evaluated the cytotoxicity of different Rg3 formulations in HUVECs and ARPE-19 cells using a CCK-8 assay. As shown in Figure S1, low concentrations of Rg3 (≤80μM) did not exhibit significant cytotoxic effects on HUVECs. In contrast, higher concentrations of Rg3 (> 80μM) reduced the

 https://doi.org/10.2147/IJN.S520756

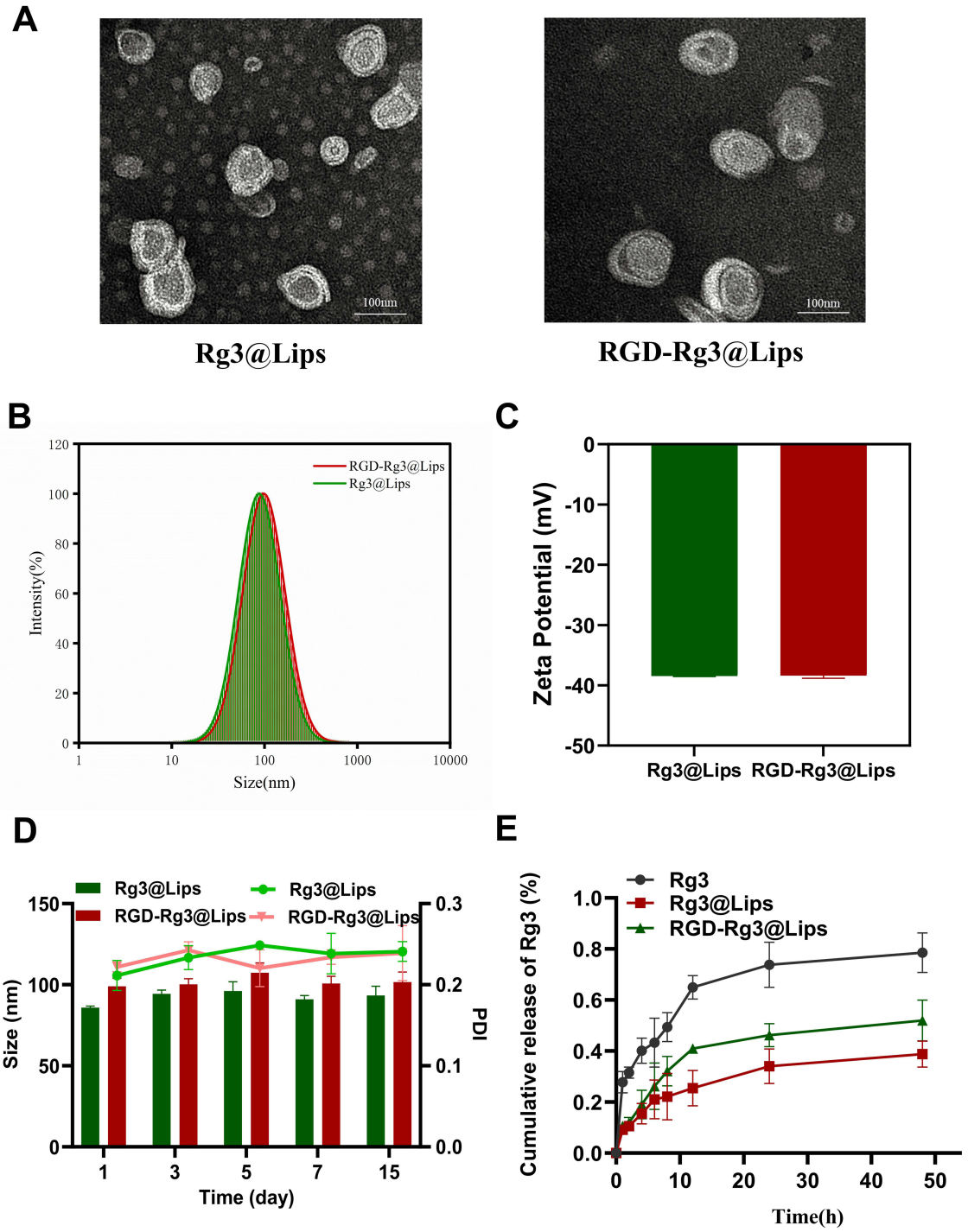

Figure 1 Preparation and characterization of Rg3@Lips and RGD-Rg3@Lips. (**A**) TEM of Rg3@Lips and RGD-Rg3@Lips. (**B**) Mean particle size of Rg3@Lips and RGD-Rg3@Lips. (**C**) Zeta-potential of Rg3@Lips and RGD- Rg3@Lips. (**D**) The changes of particle size and polydispersity index (PDI) of Rg3@Lips and RGD-Rg3@Lips stored at 4°C for 15 days (mean ± SD; n = 3). (**E**) The release profile of Rg3 from Rg3@Lips and RGD- Rg3@Lips in PBS containing 2% Tween-80 (mean ± SD; n = 3).

HUVECs viability in a dose-dependent manner. Notably, Rg3 encapsulated in the Lips (Rg3@Lips) and RGD-modified Lips (RGD-Rg3@Lips) demonstrated no apparent toxicity in HUVECs at equivalent Rg3 concentrations. These findings indicate that encapsulation mitigates Rg3-induced cytotoxicity, likely due to the sustained release of Rg3 from the Lips. Consequently, we selected 80 μM Rg3 as the working concentration for subsequent in vitro studies to minimize the potential toxicity to HUVECs. In ARPE-19 cells, as shown in Figure S2, Rg3 exhibited noticeable toxicity at

concentrations exceeding 25 μM, whereas its liposomal formulation did not induce significant toxicity at the same concentration. Therefore, 25 μM was determined to be the safe dose for ARPE-19 cells.

Given the potential influence of RGD peptide density on lip internalization efficiency, we subsequently investigated the effect of varying the ratio of DSPE-PEG-RGD to DSPE-PEG_{2000} on the cellular uptake of Lips by ARPE-19 cells. The targeting specificity of RGD-C6@Lips was assessed both quantitatively and qualitatively using flow cytometry and fluorescence microscopy. Fluorescence microscopy results revealed a significant increase in the fluorescence intensity of C6 with higher concentrations of RGD peptides (Figure 2A), suggesting that RGD modification enhanced cellular internalization of the Lips in ARPE-19 cells. Furthermore, CLSM analysis demonstrated that after 4 h of incubation, the internalization of C6@Lips was markedly higher than that of free C6, with RGD-C6@Lips exhibiting even greater uptake (Figure 2B and C). As shown in Figure 2D, the proportion of FITC-positive ARPE-19 cells was 74.41% in the C6@Lips group and 94.34% in the RGD-C6@Lips group compared to the free C6 group. These results were consistent with the flow cytometry findings, further confirming the targeting specificity of RGD-C6@Lips in the ARPE-19 cells. Additionally, we validated the ability of RGD-C6@Lips to significantly enhance C6 uptake by HUVECs through qualitative and quantitative analyses (Figure 2E and F). The substantial increase in C6 internalization following RGD modification is likely attributable to the targeted recognition of $\alpha_v\beta_3$ and $\alpha_v\beta_5$ integrin receptors, which facilitates enhanced uptake by ARPE-19 cells and HUVECs.[38,39]

RGD-Rg3@Lips Reduced Oxidative Stress in ARPE-19 Cells

RPE cells play a crucial role in maintaining retinal function, including nourishing photoreceptor cells, protecting the neural retina, removing dead cells, protecting the retina from oxidative stress, and secreting growth factors, among other functions.[40,41] Oxidative stress is a major contributor to RPE cell degeneration and is associated with AMD development. To investigate the protective effects of RGD-Rg3@Lips against oxidative damage, we used $NaIO_3$ to induce oxidative stress in ARPE-19 cells. $NaIO_3$ is a potent oxidant that is commonly used to model retinal degeneration by inducing oxidative damage in RPE cells.[42,43] As shown in Figure 3A, higher reactive oxygen species (ROS) levels were observed in the model group than in the control group, as detected using fluorescence microscopy. Compared to that in the model group, Rg3 was able to reduce the ROS production. Quantitative analysis by zymography demonstrated that Rg3@Lips further diminished ROS production compared to Rg3. Notably, RGD-Rg3@Lips exhibited the most potent ability to reduce ROS production, probably owing to enhanced cellular uptake (Figure 3B). Additionally, oxidative stress biomarkers such as MDA and SOD were assessed. Consistent with the ROS findings, Rg3 decreased MDA levels, and the liposomal formulations further amplified this effect (Figure 3C). As a major intracellular antioxidant enzyme, SOD effectively mitigated intracellular oxidative stress damage. As shown in Figure 3D, SOD activity was significantly reduced in the RPE model compared with that in the control. It was observed that the treatment with Rg3 and Lips increased the activities of SOD relative to the model group.

Studies have shown that oxidative stress can induce cellular dysfunction and apoptosis, which in turn can upregulate VEGF expression in RPE cells, thereby contributing to the formation of CNV.[44,45] We further evaluated the effects of Rg3 on VEGF secretion VEGF in $NaIO_3$ induced RPE cells. ELISA results showed a significant increase in VEGF levels 12 h after $NaIO_3$ induction compared to the control group. Treatment with Rg3 and Rg3@Lips significantly reduced VEGF levels (Figure 3E).

RGD-Rg3@Lips Attenuate HUVECs Migration and Tube Formation

VEGF produced by RPE cells is a critical factor in inducing endothelial cell proliferation and neovascularization.[46] Therefore, wound healing and tube formation assays were performed to assess the antiangiogenic effect of RGD-Rg3@Lips in vitro. HUVECs were treated with Rg3, Rg3@Lips and RGD-Rg3@Lips with Rg3 concentration of 80 μM for 4h to assess their impact on angiogenesis. The number of tubular structures and nodes was quantified and compared across the different treatment groups. The number of segments and junctions in the tube formation assay was calculated and analyzed. As shown in Figure 4A and C, compared with the control group, all three treatment groups showed inhibited tube formation. However, the anti-angiogenic effect of RGD-Rg3@Lips was significantly enhanced by RGD modification. This is likely due to the interaction between RGD peptides and integrin receptors on the surface of

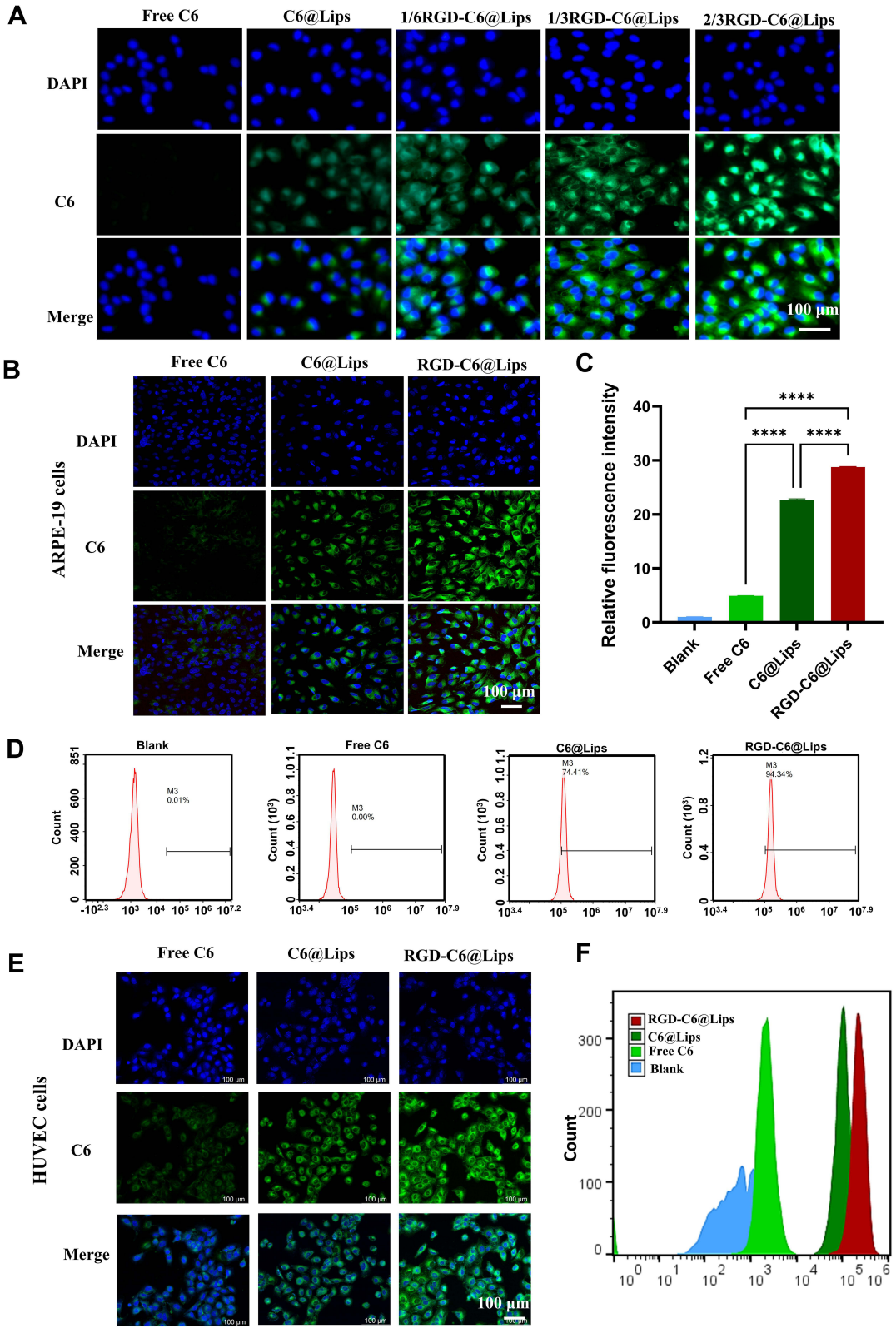

Figure 2 Analysis of nanoparticles uptake by ARPE-19 cells and HUVECs. (**A**) Fluorescence microscopy images of ARPE-19 cells incubated for 4 h with RGD-C6@Lips containing different proportions of RGD.(**B** and **E**) Fluorescence images showing cellular uptake of free C6, C6@Lips, RGD-C6@Lips in ARPE-19 cells(**B**) and HUVECs (**E**) for 4 h. (**C** and **D**) Flow cytometric histogram profiles of the fluorescence intensities for ARPE-19 cells and (**F**) HUVECs treated with free C6, C6@Lips, RGD-C6@Lips for 4 h. Mean ±SD (n = 3); ****$p < 0.0001$.

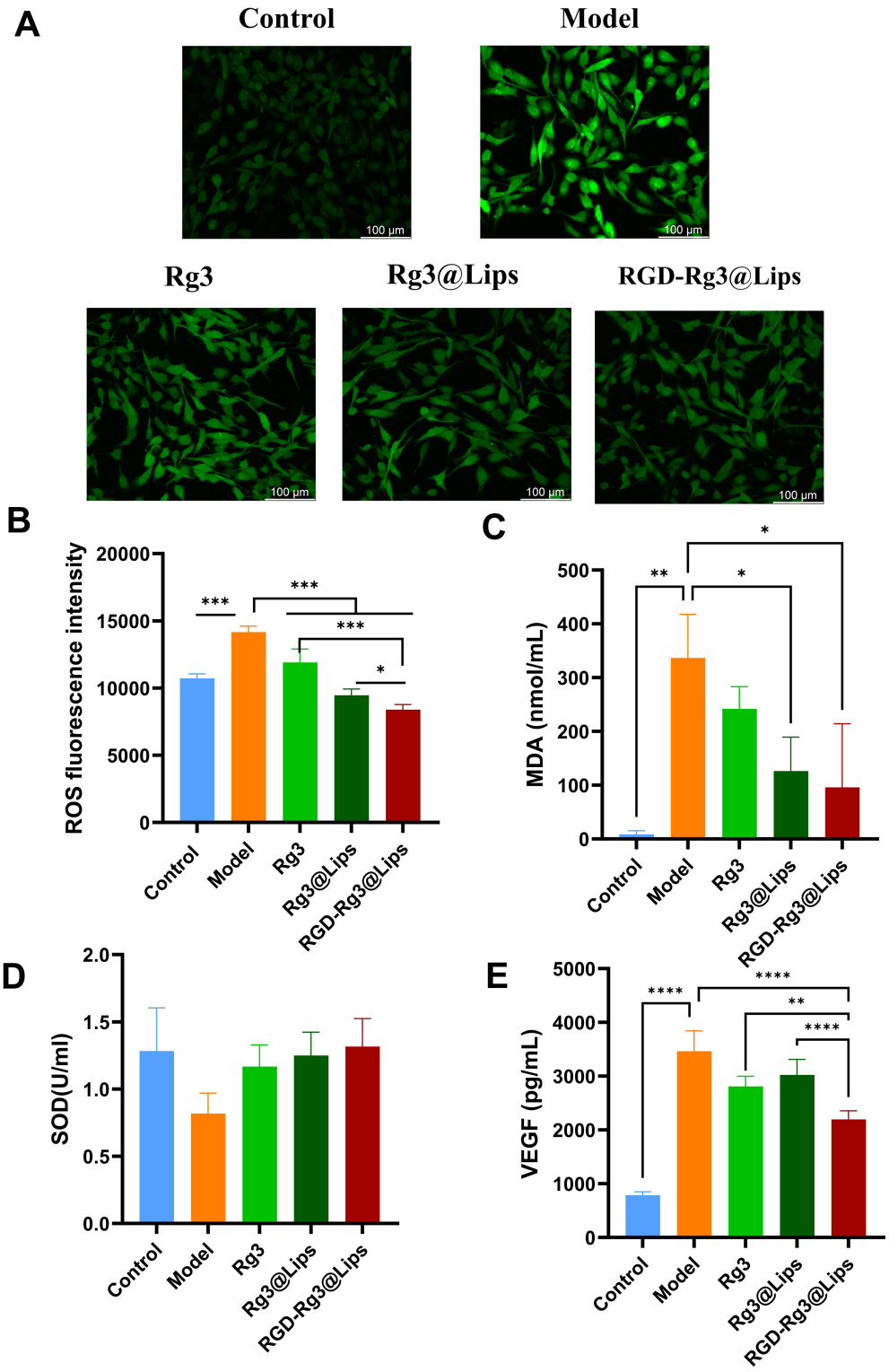

Figure 3 RGD-Rg3@Lips reduced oxidative stress in ARPE-19 cells. ARPE-19 cells were pretreated with $NaIO_3$ (6 mm) for 12 h and subsequently treated with Rg3, Rg3@Lips and RGD-Rg3@Lips for an additional 12 h. (**A** and **B**) Cells were labelled with DCFH-DA, and intracellular reactive oxygen species (ROS) levels were qualitatively analyzed by fluorescence microscopy (**A**) and quantitatively measured with a fluorescence microplate detector (**B**), respectively. The levels of (**C**) malondialdehyde (MDA), (**D**) superoxide (SOD), and (**E**) vascular endothelial growth factor (VEGF) was also measured in different groups of cells. (*p<0.05, **p< 0.01, ***p < 0.001, ****p<0.0001, n=3).

https://doi.org/10.2147/IJN.S520756

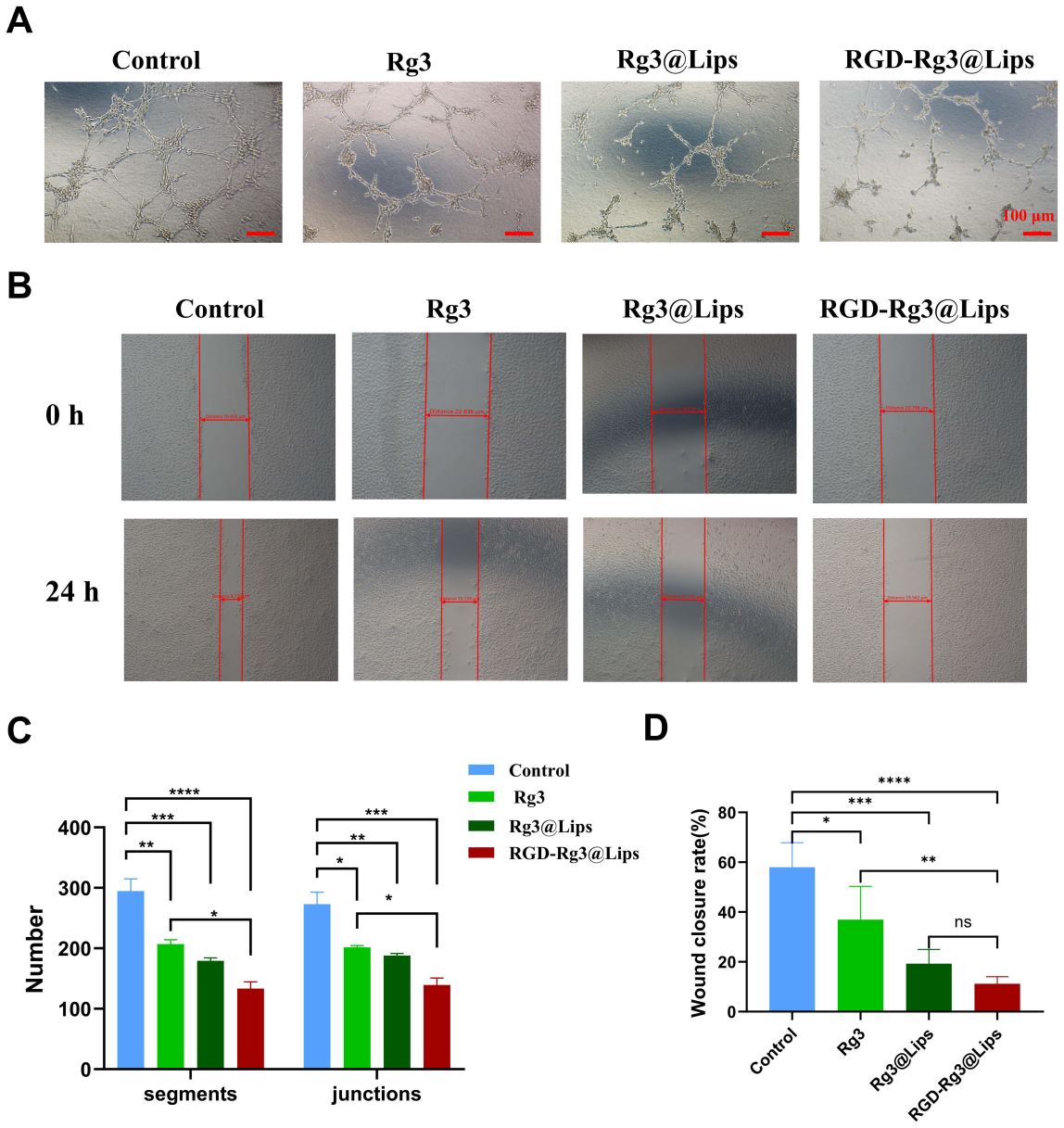

Figure 4 Anti-angiogenesis effect of Lips on HUVECs in vitro. (**A**) Tube formation assays were taken 4 h after treatment (×100 magnification). (**B**) HUVECs incubated with Rg3, Rg3@Lips and RGD-Rg3@Lips at an Rg3 concentration of 80 μM (×50 magnification). (**C**) The number of segments and junctions and (**D**) quantitative analysis of wound closure rate (*p<0.05, **p< 0.01, ***p < 0.001, ****p<0.0001, n=3).

endothelial cells, which promotes cellular uptake and inhibits angiogenesis.[34] Wound-healing assays were also performed, measuring widths at 0 h and 24 h, as illustrated in Figure 4B and D. The migration rates were calculated as (24 h-0 h)/0 h. Endothelial cell migration was faster in the control group, whereas it was significantly inhibited following 80μM RGD-Rg3@Lips. Although both Rg3 and Rg3@Lips inhibited HUVECs migration, their effects were significantly weaker than those observed with RGD-Rg3@Lips alone. This enhanced inhibition may be due to the slower release characteristics of Lips and RGD modification, which promotes cellular uptake and further impedes cell migration. The migration rates for the four groups were 0.58±0.08, 0.37±0.12, 0.19±0.05, and 0.11±0.03, respectively. The observed antiangiogenic effect of RGD-Rg3@Lips in vitro provides a foundation for subsequent in vivo experiments.

Intraocular Distribution of Lips

Although we demonstrated that the Lips exhibit excellent cellular internalization and anti-angiogenic effects in vitro, the distribution of the Lips in the vascular retinal tissues of mice remains a significant challenge. To assess whether the Lips could deliver Rg3 into mouse retinal tissues, we injected C6 and Lips into the mouse vitreous humor and evaluated their intraocular distribution. The distribution of different Lips in the mouse fundus was examined using frozen retinal sections. The results are shown in Figure 5A; green fluorescence from C6@Lips and RGD-C6@Lips was detected in both the RPE and choroid layers compared with free C6. Notably, the fluorescence intensity in the RGD-C6@Lips group was significantly higher than that in the C6@Lips group without RGD modification at 2 h. The fluorescence intensity continued to increase, showing significant enhancement at 4 h compared to that at 2 h. After 4 h IVT injection, RGD-C6 @Lips were distributed in various retinal layers, including the ganglion cell, inner nuclear, outer nuclear, and RPE layers, suggesting that RGD-modified Lips can penetrate the inner limiting membrane. In contrast, free C6 was rapidly

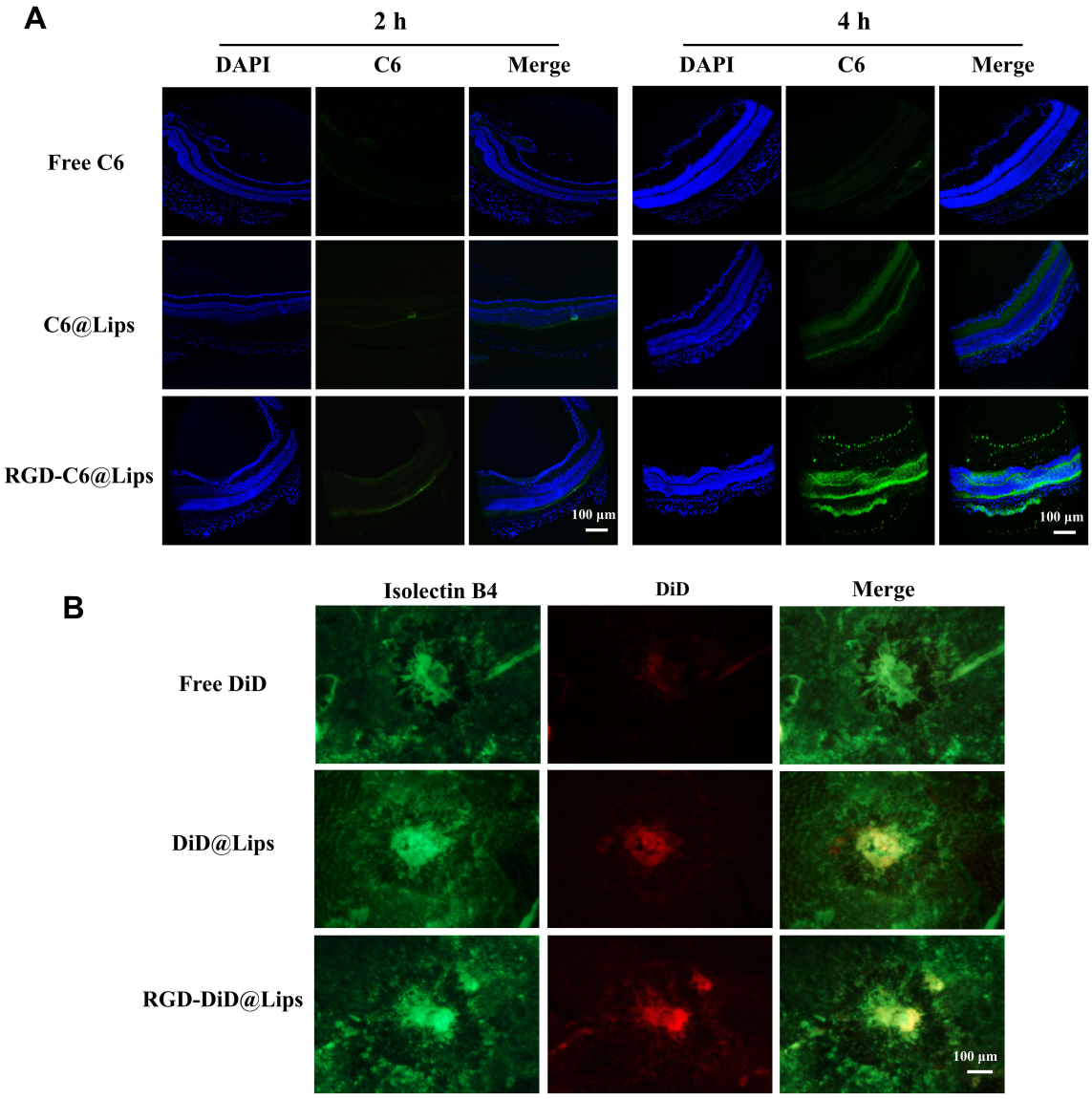

Figure 5 The distribution of Lips in the retina of mouse fundus and the ability of target CNV. (**A**) Representative fluorescence micrographs of retinal distribution of free C6, C6@Lips and RGD-C6@Lips at 2 h and 4 h after IVT injection (n=3). (**B**) The RPE/choroid/sclera fat mounts were prepared 14 d after laser injury. The fluorescence in the representative photographs indicates the localization of DiD-labeled free DiD, RGD-DiD@Lips and DiD@Lips in the isolectin B4 staining laser-induced CNV lesions (*p<0.05, **p< 0.01, ***p < 0.001, ****p<0.0001, n=3).

https://doi.org/10.2147/IJN.S520756

eliminated from the eye within 4 h, with weak fluorescence remaining, indicating that Lips modified by the RGD peptide can enhance targeting efficiency in retinal lesions.

Furthermore, we assessed the targeting ability of the RGD peptide to CNV lesion sites in mice via IVT injection of DiD-labeled Lips. CNV lesions were stained with Isolectin B4 and labeled with Alexa Fluor 488 (Figure 5B). Green fluorescence marked the CNV lesion area, whereas red fluorescence indicated accumulation of DiD-labeled Lips at the lesion site. The fluorescence intensity and fluorescence area in both the RGD-DiD@Lips and DiD@Lips groups were significantly higher than those in the free DiD group. This enhanced accumulation may be attributed to the biocompatibility of the lips, which allows easier penetration of the physiological tissue barriers to reach the lesion site. Additionally, RGD modification further promoted Lips accumulation at the CNV sites. During CNV formation, the integrin receptors, $\alpha_v\beta_3$ and $\alpha_v\beta_5$, are significantly upregulated. The specific binding of RGD to integrins at CNV sites facilitates targeted accumulation of Lips in lesions.

RGD-Rg3@Lips Suppress the Formation of CNV in vivo

The anti-angiogenic effect of RGD-Rg3@Lips was assessed in a laser-induced CNV mouse model. Laser photocoagulation induction offers advantages such as simplicity, minimal damage to the ocular surface, low cost, and a high success rate.[47] Under laser photocoagulation induction, various cytokines, chemokines, and endothelial cell adhesion molecules interact to promote CNV formation, mimicking the key factors involved in human CNV development and making it a widely used animal model for CNV.[48] To examine the pathological changes in the eyes of different mice, we performed HE staining of retinal sections. As shown in Figure 6A, large ruptures (circled in yellow) were observed throughout the fundus retina and Bruch's membrane was destroyed in the model mice. In contrast, IVT injection of Rg3@Lips and RGD-Rg3@Lips reduced the bulge around the RPE, and quantitative analysis of the CNV area showed that RGD-Rg3 @Lips had a more significant inhibitory effect on CNV growth than free Rg3. Notably, major organ sections from mice after treatment displayed no histopathological evidence of damage (Figure S3), confirming the systemic biosafety of RGD-Rg3@Lips. Hemolysis assays (Figure S4) further validated the biocompatibility of all formulations: Rg3, Rg3@Lips, and RGD-Rg3@Lips exhibited significantly lower hemolysis rates (<5%) compared to the positive control after 3 h incubation. These results highlight the formulation's dual advantage: targeted therapeutic efficacy and enhanced safety for intravitreal administration.

To further investigate the role of CNV-specific distribution in retinal drug delivery, the anti-angiogenic effect of the Lips was examined using fluorescence imaging of choroidal flat mounts stained with GS-IB4. The average neovascular area in the RGD-Rg3@Lips group was noticeably lower than that in the other three groups, which was consistent with the HE staining results, suggesting that integrin targeting is critical for improving the anti-CNV efficacy of drugs in vivo. Similarly, Rg3 and Rg3@Lips also had an inhibitory effect on CNV formation, but their effects were less pronounced than those of RGD-Rg3@Lips (Figure 6B). These results further confirm the anti-angiogenic effect of Rg3 in a laser-induced CNV mouse model. Moreover, the anti-angiogenesis effect was further enhanced by modifying the Lips with RGD, likely owing to the targeting function of the RGD peptide, which is consistent with the results of the frozen sections in Figure 5.

Integrin receptors are transmembrane heterodimeric adhesion proteins that play a crucial role in both extracellular and intracellular environments. Numerous studies have confirmed that integrin receptors are overexpressed on the surface of retinal cells and vascular endothelial cells, interacting with various cytokine-mediated signaling pathways to induce inflammation, proliferation, and migration of neovascularization in vivo.[34] RGD, a tripeptide containing arginine, glycine, and aspartate residues, has strong affinity for integrin receptors. Studies have found that exogenous RGD peptides can competitively inhibit the binding of ligands to integrins, thereby inhibiting angiogenesis and migration of tumor cells.[33] Moreover, in laser-induced CNV animal models, RGD peptide-modified nanoparticles have been shown to better deliver genes to the retinal region than unmodified nanoparticles, thereby increasing gene expression in retinal vascular endothelial cells and photoreceptor outer segments and inhibiting CNV progression.[30]

The retina is highly susceptible to oxidative stress due to factors such as high oxygen demand in the RPE, photosensitization, cumulative radiation, phagocytosis by the RPE, and polyunsaturated fatty acids in the outer segments of photoreceptor cells.[49] The accumulation of free radicals and ROS damages ocular tissues, triggering an inflammatory

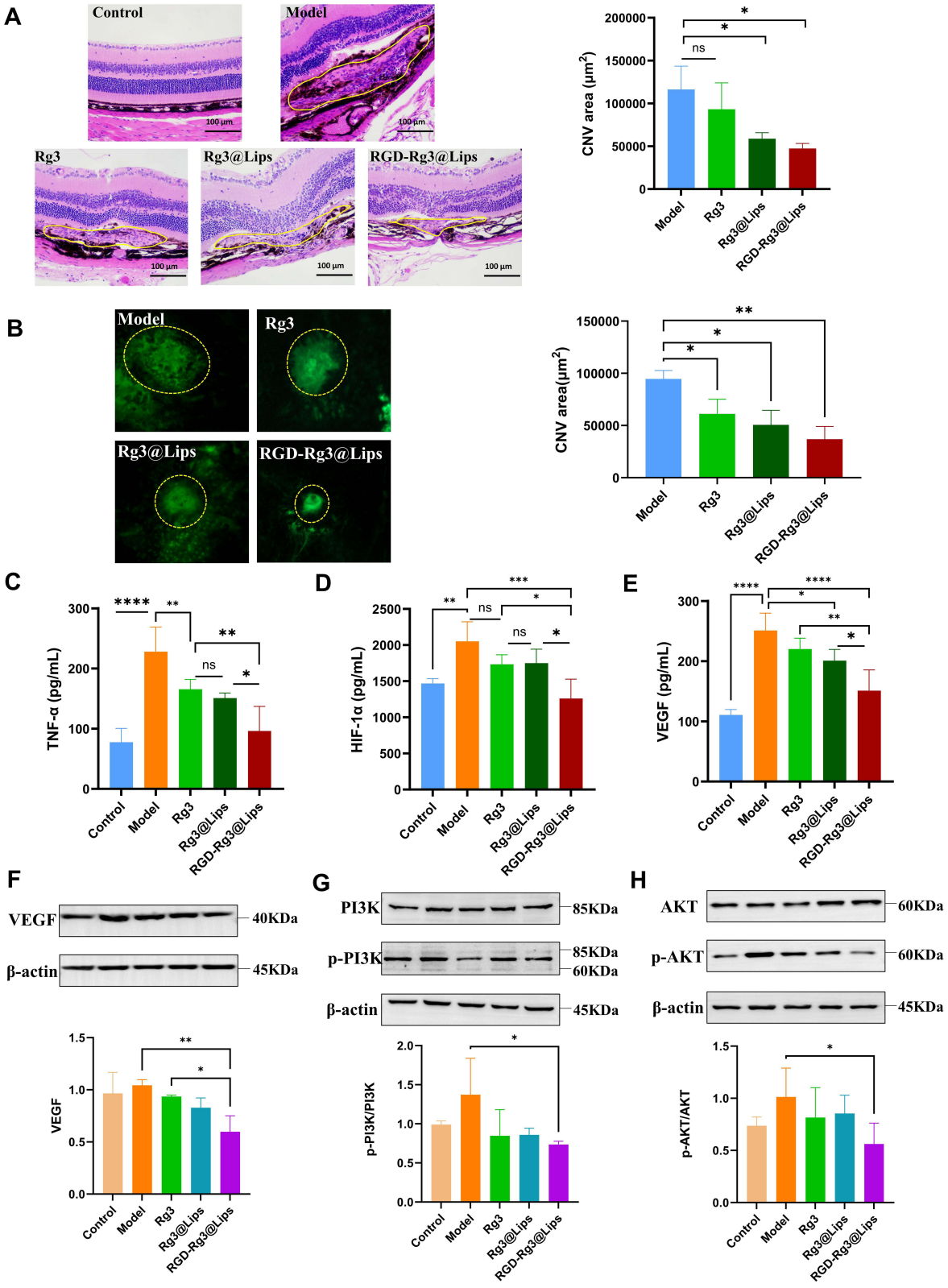

Figure 6 Effects of RGD- Rg3@Lips on retinal neovascularization in the laser-induced choroidal neovascularization (CNV) model **(A)** Representative images of HE staining of CNV lesions with the treatment of Rg3, Rg3@Lips and RGD-Rg3@Lips 14 days after photocoagulation. The yellow line indicates CNV areas. Scale bar =100 μm and quantification of the areas of CNV in pathological tissue sections (H&E staining) using ImageJ software. (n = 6) (**B**) Fluorescence micrographs of choroidal flat-mounts stained with Alexa Fluor 488-conjugated isolectin B4 on day 14 after intravitreal injection of different formulations and the mean CNV damage area after treatment of CNV mice with different preparations was calculated from the fluorescence quantified in using Image J software (n = 6). (**C**–**E**) Expression of (**C**) TNF-α, (**D**) hypoxia inducible factor-1α (HIF-1α) and (**E**) VEGF, (**F**–**H**) Western blot analysis and densitometric quantification of VEGF, p-PI3K/ PI3K, p-AKT/AKT protein levels in choroid/RPE complex. Data are mean ± SD (*p<0.05, **p< 0.01, ***p < 0.001, ****p<0.0001, ns: no significance, n = 6).

https://doi.org/10.2147/IJN.S520756

response that promotes the release of angiogenic factors such as VEGF, which play a key role in CNV formation. In vitro, we found that Rg3-loaded Lips significantly inhibited SI-induced intracellular ROS production, reduced oxidative stress levels, and decreased VEGF release in vitro. To further evaluate the anti-AMD effect of RGD-Rg3@Lips, we administered IVT injections of RGD-Rg3@Lips to the mice with laser-induced CNV. We analyzed the levels of TNF-α, HIF-1α, and VEGF in the mouse retinas. The results depicted in Figure 6C–E, indicate that the expression of TNF-α, HIF-1α, and VEGF was significantly upregulated in the model group compared to that in the healthy control group. However, following IVT treatment with Rg3@Lips and RGD-Rg3@Lips, a notable decrease in the expression of these proteins was observed in the treatment groups. Notably, the group treated with the RGD peptide-modified formulation exhibited a significant reduction in the expression of TNF-α, HIF-1α, and VEGF compared to both the unmodified lips and free drug groups.

Recent studies have confirmed the upregulation of specific cytokines in CNV tissues in both humans and animal models. Previous research has demonstrated that VEGF is overexpressed in AMD patients and laser-induced CNV animals,[50] contributing to the abnormal growth of blood vessels, characteristic of ocular neovascular diseases. Transcription of the VEGF gene in hypoxic tissues is predominantly regulated by HIF-1α, which facilitates cellular adaptation to hypoxic conditions.[50] The expression and activity of HIF-1α are closely associated with angiogenesis and retinal neovascularization.[51] Notably, CNV growth is significantly inhibited in mice with HIF-1α knockout, either pharmacologically or genetically, and is associated with downregulation of VEGF expression in ocular tissues.[52] CNV formation is also accompanied by inflammation. TNF-α, a pleiotropic cytokine, induces VEGF production in monocytes and RPE cells.[53] Additionally, TNF-α enhances the production of inflammatory cytokines by the RPE and vascular endothelial cells, thereby further promoting CNV progression. Downregulation of TNF-α in the retina has been shown to effectively inhibits diabetic retinopathy and the development of CNV and leakage. Our results also confirmed that laser-induced activation of HIF-1α, VEGF, and TNF-α in the retina with RGD-Rg3@Lips significantly downregulated the expression of these cytokines in laser-induced CNV mouse retinas, thereby inhibiting neovascularization in AMD mice. These results suggest that the downregulation of these cytokines may be a mechanism by which ginsenoside Rg3 inhibits CNV, thus presenting a potential strategy for AMD treatment. Overall, our results demonstrate that RGD-Rg3@Lips effectively attenuated oxidative stress and reduced VEGF levels in SI-induced cells and laser-induced CNV mouse models, suggesting the potential efficacy of RGD- Rg3@Lips in AMD treatment.

In addition, the serine/threonine kinase Akt plays a crucial role in cell proliferation, differentiation, and survival. It is activated by the phosphatidylinositol 3-kinase (PI3K)-dependent signaling pathway, which has been linked to pathological angiogenesis in AMD and diabetic retinopathy.[54,55] To elucidate the mechanism by which Rg3 inhibits CNV formation, we investigated the role of Rg3-loaded Lips in modulating the VEGF/PI3K/AKT signaling pathway. Our findings showed that exposure to a 532 nm laser resulted in increased phosphorylation of the 85-kDa protein (p85) associated with VEGF, AKT, and PI3K in the mouse retina. This upregulation was effectively suppressed by the IVT administration of RGD-Rg3@Lips (Figure 6F–H). Overall, our results suggest that RGD-Rg3@Lips may improve laser-stimulated retinal angiogenesis by targeting the vascular endothelium to inhibit the VEGF-regulated PI3K/AKT signaling pathway.

Conclusions

The findings of this study demonstrate that RGD-Rg3@Lips effectively target integrin receptors at CNV lesions, aligning with recent advances in nanomedicine for ocular diseases. For instance, supramolecular-engineered nanoceria systems have similarly leveraged multifunctional designs to address oxidative stress in AMD, underscoring the importance of dual-targeted strategies. Our results corroborate emerging evidence that lipid-based carriers with active targeting moieties enhance therapeutic precision compared to passive delivery systems. Mechanistically, the inhibition of HIF-1α/VEGF and PI3K/AKT pathways by RGD-Rg3@Lips mirrors findings from studies on bioactive hydrogels for corneal repair, where localized drug retention critically influenced therapeutic outcomes. However, unlike hydrogel-based systems optimized for anterior segment delivery, our liposomal platform prioritizes posterior segment penetration—a key challenge in AMD therapy.

In conclusion, this study presents RGD-Rg3@Lips as a multitargeted therapeutic strategy for AMD, combining the natural compound Rg3's antioxidant/anti-angiogenic properties with integrin-directed liposomal delivery. The formulation's small size and negative charge facilitated enhanced retinal distribution and cellular uptake. This targeted delivery ensures superior therapeutic efficacy, including the reduction of oxidative stress and inhibition of inflammation, thereby modifying the CNV microenvironment. Mechanistic investigations revealed that RGD-Rg3@Lips attenuated oxidative stress and inhibited the HIF-1α/VEGF signaling pathway. In a laser-induced animal model of AMD, the IVT injection of RGD-Rg3@Lips significantly ameliorated the expression of inflammatory factors and markedly reduced the progression of neovascularization and vascular leakage. This retina-targeted modulation therapy, based on multi-targeting of natural products, including ROS scavenging, anti-inflammatory effects, and regulation of the VEGF/PI3K/AKT signaling pathway, demonstrated excellent anti-AMD effects.

Despite these advances, limitations must be acknowledged. In this study, we observed that IVT injection of RGD-Rg3 @Lips improved drug distribution within the retina and exhibited anti-AMD effects at both cellular and animal levels. However, the efficacy of non-invasive administration methods, such as eye drops, remains further to be evaluated. Additionally, the safety and long-term efficacy of this drug require further investigation. This study remains at the exploratory laboratory stage and necessitates more comprehensive research, testing, and optimization to ensure the maturity and reliability of the technology, ultimately facilitating the clinical translation of these findings.

Ethics Approval and Consent to Participate

All animal experimental protocols were approved by the Institutional Animal Care and Use Committee of Chengdu University and conformed to the National Institutes of Health (NIH) guidelines.

Author Contributions

All authors made a significant contribution to the work reported, whether that is in the conception, study design, execution, acquisition of data, analysis and interpretation, or in all these areas; took part in drafting, revising or critically reviewing the article; gave final approval of the version to be published; have agreed on the journal to which the article has been submitted; and agree to be accountable for all aspects of the work.

Funding

This work was supported by the National Natural Science Foundation of China (82405202; 82274372) and Natural Science Foundation of Sichuan Province (2023NSFSC1785). This study was supported by the Open Research Fund of Chengdu University of Traditional Chinese Medicine State Key Laboratory of Southwestern Chinese Medicine Resources (SKLTCM202209) and Open Project of Sichuan Provincial Key Laboratory for Human Disease Gene Study (2023kflx002).

Disclosure

The authors declare that they have no competing interests.

References

1. Wong WL, Su X, Li X, et al. Global prevalence of age-related macular degeneration and disease burden projection for 2020 and 2040: a systematic review and meta-analysis. *Lancet Global Health*. 2014;2(2):e106–e116. doi:10.1016/S2214-109X(13)70145-1
2. Song P, Du Y, Chan KY, et al. The national and subnational prevalence and burden of age–related macular degeneration in China. *J Glob Health*. 2017;7(2):020703.
3. Fernandes AR, Zielińska A, Sanchez-Lopez E, et al. Exudative versus nonexudative age-related macular degeneration: physiopathology and treatment options. *Int J Mol Sci*. 2022;23(5):2592. doi:10.3390/ijms23052592
4. Patel P, Sheth V. New and innovative treatments for neovascular Age-Related Macular Degeneration (nAMD). *J Clin Med*. 2021;10(11):12. doi:10.3390/jcm10112436
5. Blasiak J. Senescence in the pathogenesis of age-related macular degeneration. *Cell Mol Life Sci*. 2020;77:789–805. doi:10.1007/s00018-019-03420-x
6. Shao Y, Yu H, Yang Y, et al. A solid dispersion of quercetin shows enhanced Nrf2 activation and protective effects against oxidative injury in a mouse model of dry age-related macular degeneration. *Oxid Med Cell Longevity*. 2019;2019(1):1479571. doi:10.1155/2019/1479571
7. Rozing MP, Durhuus JA, Nielsen MK, et al. Age-related macular degeneration: a two-level model hypothesis. *Prog Retinal Eye Res*. 2020;76:100825 doi:10.1016/j.preteyeres.2019.100825.

8. Mason JO, Colagross CC, Feist RM, et al. Risk factors for severe vision loss immediately after transpupillary thermotherapy for occult subfoveal choroidal neovascularization. *Ophthalmic Surg Lasers Imaging Retina*. 2008;39(6):460–465. doi:10.3928/15428877-20081101-09
9. Hamdi HK, Kenney C. Age-related macular degeneration: a new viewpoint. *Front Biosci*. 2003;8:e305–e314. doi:10.2741/1019
10. Cohen SY, Oubraham H, Uzzan J, et al. Causes of unsuccessful ranibizumab treatment in exudative age-related macular degeneration in clinical settings. *Retina*. 2012;32(8):1480–1485. doi:10.1097/IAE.0b013e318240a516
11. Hussain RM, Ciulla TA. Treatment strategies for refractory diabetic macular edema: switching anti-VEGF treatments, adopting corticosteroid-based treatments, and combination therapy. *Expert Opin Biol Ther*. 2016;16(3):365–374. doi:10.1517/14712598.2016.1131265
12. Hashida N, Nishida K. Recent advances and future prospects: current status and challenges of the intraocular injection of drugs for vitreoretinal diseases. *Adv Drug Deliv Rev*. 2023;198:114870. doi:10.1016/j.addr.2023.114870
13. Kaarniranta K, Blasiak J, Liton P, et al. Autophagy in age-related macular degeneration. *Autophagy*. 2023;19(2):388–400. doi:10.1080/15548627.2022.2069437
14. Fini ME, Schwartz SG, Gao X, et al. Steroid-induced ocular hypertension/glaucoma: focus on pharmacogenomics and implications for precision medicine. *Prog Retinal Eye Res*. 2017;56:58–83 doi:10.1016/j.preteyeres.2016.09.003..
15. Li W, Chen L, Gu Z, et al. Co-delivery of microRNA-150 and quercetin by lipid nanoparticles (LNPs) for the targeted treatment of age-related macular degeneration (AMD). *J Control Release*. 2023;355:358–370. doi:10.1016/j.jconrel.2023.01.080
16. Lewis Luján LM, Mccarty MF, Di Nicolantonio JJ, et al. Nutraceuticals/drugs promoting mitophagy and mitochondrial biogenesis may combat the mitochondrial dysfunction driving progression of dry age-related macular degeneration. *Nutrients*. 2022;14(9):1985. doi:10.3390/nu14091985
17. Shivarudrappa AH, Ponesakki G. Lutein reverses hyperglycemia-mediated blockage of Nrf2 translocation by modulating the activation of intracellular protein kinases in retinal pigment epithelial (ARPE-19) cells. *J Cell Commun Signaling*. 2020;14(2):207–221. doi:10.1007/s12079-019-00539-1
18. Wang J, Zeng L, Zhang Y, et al. Pharmacological properties, molecular mechanisms and therapeutic potential of ginsenoside Rg3 as an antioxidant and anti-inflammatory agent. *Front Pharmacol*. 2022;13:975784. doi:10.3389/fphar.2022.975784
19. Ren B, Feng J, Yang N, et al. Ginsenoside Rg3 attenuates angiotensin II-induced myocardial hypertrophy through repressing NLRP3 inflammasome and oxidative stress via modulating SIRT1/NF-κB pathway. *Int Immunopharmacol*. 2021;98:107841. doi:10.1016/j.intimp.2021.107841
20. Nakhjavani M, Smith E, Townsend AR, et al. Anti-angiogenic properties of ginsenoside Rg3. *Molecules*. 2020;25(21):4905. doi:10.3390/molecules25214905
21. Liang Y, Zhang T, Jing S, et al. 20 (S)-ginsenoside Rg3 inhibits lung cancer cell proliferation by targeting EGFR-mediated Ras/Raf/MEK/ERK pathway. *Am J Chin Med*. 2021;49(03):753–765. doi:10.1142/S0192415X2150035X
22. Huang Y, Lu J, Zhao L, et al. Retinal cell-targeted liposomal ginsenoside Rg3 attenuates retinal ischemia-reperfusion injury via alleviating oxidative stress and promoting microglia/macrophage M2 polarization. *Free Radic Biol Med*. 2023;206:162–179. doi:10.1016/j.freeradbiomed.2023.06.024
23. Sun H-Q, Zhou Z-Y. Effect of ginsenoside-Rg3 on the expression of VEGF and TNF-α in retina with diabetic rats. *Int J Ophthalmol*. 2010;3(3):220. doi:10.3980/j.issn.2222-3959.2010.03.09
24. Han H, Li S, Xu M, et al. Polymer- and lipid-based nanocarriers for ocular drug delivery: current status and future perspectives. *Adv Drug Deliv Rev*. 2023;196:114770. doi:10.1016/j.addr.2023.114770
25. Xu M, Zhou Y, Xu Y, et al. Supramolecular engineering of nanoceria for management and amelioration of age-related macular degeneration via the two-level blocking of oxidative stress and inflammation. *Adv Sci*. 2025;12(9):e2408436. doi:10.1002/advs.202408436
26. Huang J, Jiang T, Qie J, et al. Biologically inspired bioactive hydrogels for scarless corneal repair. *Sci Adv*. 2024;10(51):eadt1643. doi:10.1126/sciadv.adt1643
27. Nandrot EF, Kim Y, Brodie SE, et al. Loss of synchronized retinal phagocytosis and age-related blindness in mice lacking αvβ5 integrin. *J Exp Med*. 2004;200(12):1539–1545. doi:10.1084/jem.20041447
28. Finnemann SC. Role of αvβ5 integrin in regulating phagocytosis by the retinal pigment epithelium. *Retinal Degeneration*. 2003;2003:337–342 doi:10.1007/978-1-4615-0067-4_42.
29. Chu Y, Chen N, Yu H, et al. Topical ocular delivery to laser-induced choroidal neovascularization by dual internalizing RGD and TAT peptide-modified nanoparticles. *Int J Nanomed*. 2017;Volume 12:1353–1368. doi:10.2147/IJN.S126865
30. Singh S, Grossniklaus H, Kang S, et al. Intravenous transferrin, RGD peptide and dual-targeted nanoparticles enhance anti-VEGF intraceptor gene delivery to laser-induced CNV. *Gene Ther*. 2009;16(5):645–659. doi:10.1038/gt.2008.185
31. Zhou X, Liu H-Y, Zhao H, et al. RGD-modified nanoliposomes containing quercetin for lung cancer targeted treatment. *Oncol Targets Ther*. 2018;11:5397–5405. doi:10.2147/ott.S169555
32. Zhang J, Zhu J, Zhao L, et al. RGD-modified multifunctional nanoparticles encapsulating salvianolic acid A for targeted treatment of choroidal neovascularization. *J Nanobiotechnol*. 2021;19(1). doi:10.1186/s12951-021-00939-9
33. Chen C-W, Yeh L, Yeh MK, Shiau CY, Chiang CH. Novel RGD-lipid conjugate-modified liposomes for enhancing siRNA delivery in human retinal pigment epithelial cells. *Int J Nanomed*. 2011;2011:2567. doi:10.2147/ijn.S24447
34. Van Hove I, Hu -T-T, Beets K, et al. Targeting RGD-binding integrins as an integrative therapy for diabetic retinopathy and neovascular age-related macular degeneration. *Prog Retinal Eye Res*. 2021;85:100966 doi:10.1016/j.preteyeres.2021.100966.
35. Chen C-W, Yeh M-K, Shiau C-Y, et al. Efficient downregulation of VEGF in retinal pigment epithelial cells by integrin ligand-labeled liposome-mediated siRNA delivery. *Int J Nanomed*. 2013;2013:2613–2627 doi:10.2147/IJN.S39622.
36. Ramsay E, Lajunen T, Bhattacharya M, et al. Selective drug delivery to the retinal cells: biological barriers and avenues. *J Control Release*. 2023;361:1–19. doi:10.1016/j.jconrel.2023.07.028
37. Xia J, Chen C, Dong M, et al. Ginsenoside Rg3 endows liposomes with prolonged blood circulation and reduced accelerated blood clearance. *J Control Release*. 2023;364:23–36. doi:10.1016/j.jconrel.2023.10.023
38. Friedlander M, Theesfeld CL, Sugita M, et al. Involvement of integrins alpha v beta 3 and alpha v beta 5 in ocular neovascular diseases. *Proc Natl Acad Sci*. 1996;93(18):9764–9769. doi:10.1073/pnas.93.18.9764
39. Millard M, Odde S, Neamati N. Integrin targeted therapeutics. *Theranostics*. 2011;1:154. doi:10.7150/thno/v01p0154
40. Wang S, Li W, Chen M, et al. The retinal pigment epithelium: functions and roles in ocular diseases. *Fundam res*. 2023;2023:1 doi:10.1016/j.fmre.2023.08.011.

41. Kinnunen K, Petrovski G, Moe MC, et al. Molecular mechanisms of retinal pigment epithelium damage and development of age-related macular degeneration. *Acta Ophthalmol*. 2012;90(4):299–309. doi:10.1111/j.1755-3768.2011.02179.x
42. Liu B, Wang W, Shah A, et al. Sodium iodate induces ferroptosis in human retinal pigment epithelium ARPE-19 cells. *Cell Death Dis* 2021;12 (3):230. doi:10.1038/s41419-021-03520-2
43. Chen W, Ye Y, Wu Z, et al. Temporary upregulation of Nrf2 by naringenin alleviates oxidative damage in the retina and ARPE-19 cells. *Oxid Med Cell Longevity*. 2021;2021(1):4053276. doi:10.1155/2021/4053276
44. Salimiaghdam N, Riazi-Esfahani M, Fukuhara PS, et al. Age-related macular degeneration (AMD): a review on its epidemiology and risk factors. *Open Ophthalmol J*. 2019;13(1):90–99. doi:10.2174/1874364101913010090
45. Finger RP, Puth M-T, Schmid M, et al. Lifetime outcomes of anti–vascular endothelial growth factor treatment for neovascular age-related macular degeneration. *JAMA Ophthalmol*. 2020;138(12):1234–1240. doi:10.1001/jamaophthalmol.2020.3989
46. Ranjbar M, Brinkmann MP, Tura A, et al. Ranibizumab interacts with the VEGF-A/VEGFR-2 signaling pathway in human RPE cells at different levels. *Cytokine*. 2016;83:210–216. doi:10.1016/j.cyto.2016.04.014
47. Hara C, Kasai A, Gomi F, et al. Laser-induced choroidal neovascularization in mice attenuated by deficiency in the apelin-APJ system. *Invest Ophthalmol Visual Sci*. 2013;54(6):4321–4329. doi:10.1167/iovs.13-11611
48. Yamada K, Sakurai E, Itaya M, et al. Inhibition of laser-induced choroidal neovascularization by atorvastatin by downregulation of monocyte chemotactic protein-1 synthesis in mice. *Invest Ophthalmol Visual Sci*. 2007;48(4):1839–1843. doi:10.1167/iovs.06-1085
49. Wojciechowski AM, Bell BA, Song Y, et al. Inducible RPE-specific GPX4 knockout causes oxidative stress and retinal degeneration with features of age-related macular degeneration. *Exp Eye Res*. 2024;247:110028. doi:10.1016/j.exer.2024.110028
50. Zhao T, Zhang J, Zhang Y, et al. Vascular endothelial growth factor receptor 2 antibody, BC001, attenuates laser-induced choroidal neovascularization in rhesus monkeys (Macaca mulatta). *J Ocul Pharmacol Ther*. 2015;31(10):611–616. doi:10.1089/jop.2014.0148
51. Luhmann UF, Lin J, Acar N, et al. Role of the Norrie disease pseudoglioma gene in sprouting angiogenesis during development of the retinal vasculature. *Invest Ophthalmol Visual Sci*. 2005;46(9):3372–3382. doi:10.1167/iovs.05-0174
52. Yoshida T, Zhang H, Iwase T, et al. Digoxin inhibits retinal ischemia-induced HIF-1α expression and ocular neovascularization. *FASEB J*. 2010;24 (6):1759. doi:10.1096/fj.09-145664
53. W-H C, Chen Y, Cui G-H. Effects of TNF-α and curcumin on the expression of VEGF in Raji and U937 cells and on angiogenesis in ECV304 cells. *Chin Med J*. 2005;118(24):2052–2057.
54. Yang X-M, Wang Y-S, Zhang J, et al. Role of PI3K/Akt and MEK/ERK in mediating hypoxia-induced expression of HIF-1α and VEGF in laser-induced rat choroidal neovascularization. *Invest Ophthalmol Visual Sci*. 2009;50(4):1873–1879. doi:10.1167/iovs.08-2591
55. Wang L, Liu W-X, Huang X-G. MicroRNA-199a-3p inhibits angiogenesis by targeting the VEGF/PI3K/AKT signalling pathway in an in vitro model of diabetic retinopathy. *Exp Mol Pathol*. 2020;116:104488. doi:10.1016/j.yexmp.2020.104488